Volume 1 | Number 1 | Jan 2013 | Pages 1–100

Journal of
Materials Chemistry A

Materials for energy and sustainability
www.rsc.org/materialsA

Li⁺

ROYAL SOCIETY OF CHEMISTRY

ROYAL SOCIETY OF CHEMISTRY

www.rsc.org/materialsA

Journal Name

ARTICLE

Si-based nanocomposites derived from layered CaSi₂: Influence of synthesis conditions on composition and anode performance in Li ion batteries.

Song-Yul Oh,*[a] Haruo Imagawa[a] and Hiroshi Itahara**[a]

Various Si-based nanocomposites consisting of nanoflake-like Ca_xSi_2 particles and transition metal silicide (MSi_y) particles were synthesized by a solid-state exfoliation reaction using layered $CaSi_2$ and transition metal (M) chlorides (M: Ni, Fe or Mn). $CaCl_2$ was found to form in all samples irrespective of the chloride used. Based on the shape and composition of the nanocomposites, it is thought that Ca_xSi_2 particles were formed by extraction of Ca from the layered $CaSi_2$. The molar ratio of $CaSi_2$ and $NiCl_2$ and the synthesis temperature were systematically varied to investigate their influence on the characteristics of the reaction products, e.g. crystalline phases, microstructure, anode capacity as lithium-ion batteries and electrical conductivity. Nanocomposites with various mixtures of Ca_xSi_2 particles (Li storage sites) and $NiSi_y$ particles (conducting media) were formed. The synthesized samples showed a wide range of electrical properties depending on the composition. For example, sample exhibited an anode capacity and an electrical conductivity of 1,020 mAh g^{-1} and 6×10^{-8} S cm^{-1}, and another 479 mAh g^{-1} and 2×10^{-5} S cm^{-1}, respectively. Because of its simplicity, the solid-state exfoliation reaction using layered $CaSi_2$ and MCl_2 provides a facile and scalable method to synthesize Si-based nanocomposite anode materials for lithium ion batteries.

Introduction

Silicon and Si-based materials are expected to be alternate candidates for anode materials in lithium-ion batteries (LIBs)[1, 2]. They are some of the highest capacity anode materials[1]. However, large capacity fading, caused by cracking of Si particles and detachment from the current collector due to the large volume change during charge/discharge (or lithiation/delithiation) cycles, hinders their practical application. To overcome these problems, nanostructured Si-based materials, such as porous nanoparticles and nanotubes, have been suggested[3-8]. Since these contain an inner hollow space that can facilitate a reversible volume change of Si during charge/discharge cycles, such materials have been reported to show stable cyclability without significant capacity fading. So-called templating methods using various materials, such as small SiO_2 particles[3, 7, 8], polymer fibers[7, 8] and anodized Al_2O_3[9] are commonly adopted to fabricate such nano-structured materials. Since the templates used need to be removed, the synthesis process is complicated and the yield of the final products is still low.

We previously reported a synthesis method for producing Si-based nanocomposites, which is the solid-state exfoliation reaction using layered $CaSi_2$ as the raw substance[10]. For example, nanocomposites containing nano-flake particles with compositions close to Si, and iron silicide particles ($FeSi_z$: e.g., $FeSi$, Fe_3Si) were synthesized by a reaction between $CaSi_2$ and $FeCl_2$. In particular, the nano-flakes had a thickness of around

10 nm and they were stacked with gaps of a few nanometers between them. It was considered that the nano-flake particles were formed by extraction of Ca from layered-$CaSi_2$ and exfoliation of the layered structure[10, 11]. These are hereafter designated as Ca_xSi_2. The nanocomposite containing $FeSi_z$ and Ca_xSi_2 showed higher capacity than conventional graphite. Because $FeSi_z$ hardly reacts with Li, Ca_xSi_2 would act as Li-storage sites[10] and $FeSi_z$ would work as the conductive medium.

On the other hand, to enhance the cyclability of Si-based anodes during charge/discharge cycles, composite electrode materials containing conductive additives such as silicides or other electrical conducting materials (e.g., carbon, TiN, SiC) were investigated[4, 7, 12]. These conducting materials maintain the conduction paths between Li-storage sites and the current collector during charge/discharge cycles. Therefore, control of the composition ratio and the microstructure of the nanocomposites are essential in order to develop high performance anodes with cyclability.

In the present study, we applied our proposed solid-state exfoliation reaction[10, 11] to the synthesis of nanocomposites containing nano-flake structured Ca_xSi_2 (Li-storage site) and silicides (conductive medium) under various synthesis conditions, aiming to control the composition and microstructure. A mixture of $NiCl_2$ and layered $CaSi_2$ was used as a model system, and the crystal structure and microstructure of the reaction products were analyzed. The synthesis temperature (T_{syn}) and molar ratio (α) for $NiCl_2$ and layered $CaSi_2$ were systematically changed. We compared the

relationships among the compositions, anode capacity and electrical conductivity of the synthesized samples. We also prepared nanocomposites using a mixture of 'FeCl$_2$ and CaSi$_2$' and 'MnCl$_2$ and CaSi$_2$' for comparison.

Experimental

Reagent-grade anhydrous NiCl$_2$ (Kojundo Chemical Lab. Co., Ltd.) and CaSi$_2$ (Rare Metallic Co., Ltd.) were used as the raw substances. The synthesis procedure and characterization methods were similar to those described in previous work[10, 11].

Table 1. Summary of synthesis conditions for αNiCl$_2$/CaSi$_2$ systems.

| Sample | T_{syn} /°C | Raw materials / mg | | α^a / - |
		NiCl$_2$	CaSi$_2$	
T1	250			
T2	300			
T3	350	150	56	2.0
T4	400			
T5	500			
T6(A1)				
A2		140	65	1.6
A3		130	73	1.3
A4	600	130	85	1.1
A5		115	85	1.0
A6		95	105	0.7
A7		85	126	0.5

note: a is molar ratio of (NiCl$_2$/CaSi$_2$).

As summarized in Table 1, a predetermined amount of mixed raw substances (~200 mg) was packed inside a boron nitride (BN) pot. Each BN pot was set inside a stainless-steel closed cell in an Ar atmosphere under ambient pressure. The samples were prepared under various conditions: the molar ratio (α) of NiCl$_2$ and CaSi$_2$ was varied in the range of 0.5-2.0 and the synthesis temperature (T_{syn}) was set in the range of 250-600°C (a heating rate of 100°C h^{-1} and a holding time of 5 h were used). The synthesized samples were washed with anhydrous dimethylformamide (DMF; Wako Pure Chemical Industries, Ltd.), followed by vacuum drying at 80°C overnight. For comparison, reagent-grade anhydrous FeCl$_2$ or MnCl$_2$ (Kojundo Chemical Lab. Co., Ltd.) was used instead of NiCl$_2$. The samples were prepared at 600°C with an α of 1.0 for the 'FeCl$_2$ and CaSi$_2$' system and an α of 0.5 for the 'MnCl$_2$ and CaSi$_2$' system in the same manner.

The crystalline phases and microstructure of the samples were analyzed by powder X-ray diffraction (XRD; RINT-1500V, Rigaku) and scanning electron microscopy (SEM; SU3500, Hitachi).

The anode capacity was evaluated using a galvanostat (HJ1010mSM8; Hokuto Denko Corp.). Electrodes were prepared by mixing the samples and carbon black with a nominal weight ratio of 70 to 30, followed by pressing onto a Ni-form at 10 MPa for 3 min. A Li foil was used as the counter/reference electrode and 1 M-LiPF$_6$ dissolved in a mixture of ethylene carbonate/diethyl carbonate (EC/DEC; 50/50 vol%) was used as the electrolyte solution. A constant current of 100 mA g^{-1} was applied with a voltage window of 0.02-1.50 V vs. Li/Li$^+$.

The electrical conductivity (σ) of the synthesized powders was measured as follows. The synthesized powders were set inside an insulating mold. Conductivity (σ) values were evaluated using the two-probe method while the powders were uniaxially pressed under loading in the range of 2-15 MPa. A dc current between $\pm 10^{-7}$ and ± 1.0 A was applied.

Results and discussion

(1) Influence of synthesis conditions on crystalline phase and microstructure of the nanocomposites

SEM images of samples A5 (α=1.0) and A3 (α=1.3) synthesized at 600°C are shown in Figure 1(a) and 1(b), respectively, as typical examples. Sample A5 was an agglomerated powder, consisting of large particles with diameters of 10-20 μm (Figure 1(a-2)) and small particles with diameters around 1 μm. Elemental analysis using energy dispersive spectroscopy (EDS) indicated that the former and latter were respectively particles consisting of 'Ca and Si (around 0.1 to 2.0 atomic ratio)', and 'Ni'. In particular, similar to our previous reports[10, 11], large particles were composed of nano-flake particles, which are stacked with small gaps as shown in Fig.1(a-3). These particles are believed to be Ca$_x$Si$_2$, derived from exfoliation of the layered CaSi$_2$ upon extracting Ca from CaSi$_2$ with CaCl$_2$ formation as driving force of the reaction[10, 11]. For sample A3 (α=1.3; Figure 1(b)), the SEM image indicates only agglomerated small particles with sizes of around 1 μm, wherein Ca$_x$Si$_2$ particles were not observed. SEM images suggested that samples A7, A6, A5 and A4 included Ca$_x$Si$_2$ particles while samples A3, A2 and T6(A1) did not include Ca$_x$Si$_2$. For the sample containing Ca$_x$Si$_2$ particles, specific surface areas are increased with increasing α values (see SEI, Table S1 and Fig. S1), suggesting the smaller sizes of Ca$_x$Si$_2$. These results are reasonable because the Ca extraction reaction with CaCl$_2$ formation would be more favorable with larger amount of NiCl$_2$ (*i.e.*, larger α values).

On the other hand, samples T1-T3 synthesized with T_{syn} between 250 and 350°C contained Ca$_x$Si$_2$ particles similar to those in sample A5 (Figure 1(a)), whereas samples T4-T6(A1) synthesized at higher T_{syn} between 400 and 600°C consisted only of agglomerated small particles with sizes of around 1 μm (*i.e.*, no Ca$_x$Si$_2$ particles), similar to sample A3 (Figure 1(b)). The small particles were Nickel silicide which is formed by the reaction of Ca$_x$Si$_2$ and Ni as described below (see, Fig.2 and Table 2). Particles sizes of Ca$_x$Si$_2$ are expected to be smaller with increasing T_{syn}. This is because both Ca extraction from CaSi$_2$ and formation of Nickel silicide (i.e. consumption of Ca$_x$Si$_2$) are considered to be more favorable for higher T_{syn}.
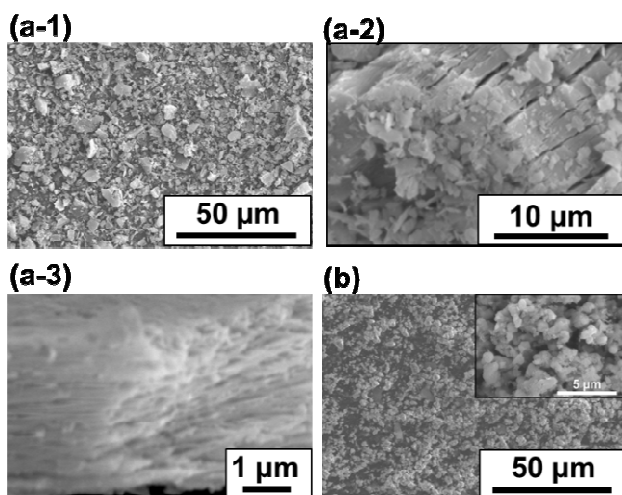
Figure 1. SEM images of DMF-washed samples synthesized at 600°C. (a) and (b) show sample A5 (α=1.0) and A3 (α=1.3), respectively. The inset of (b) is higher magnification image. (a-2) and (a-3) show SEM images for Ca$_x$Si$_2$ particles.

According to powder XRD analysis, the raw CaSi$_2$ contained traces of Si and CaSi. XRD patterns for samples synthesized with T_{syn} lower than 200°C were similar to those for the raw mixture; no peaks corresponding to the reaction products were observed. Peaks corresponding to CaCl$_2$ were clearly observed in the patterns for all samples ($T_{syn} \geq 250$°C) before washing with DMF. These peaks were not observed for the samples after washing.

In Figure 2(a), XRD patterns for the samples synthesized with fixed α=2.0 at various T_{syn} in the range of 250-600°C are shown. In the XRD pattern for sample T1 (T_{syn}=250°C), peaks associated with Ni and raw CaSi$_2$ were identified. From the pattern for sample T2 (T_{syn}=300°C), the crystalline material is only Ni, and no peaks corresponding to the raw substances were observed. In contrast, peaks corresponding to Ni and/or nickel silicides (NiSi$_y$) were observed as the major crystalline phases from the patterns for the samples synthesized at T_{syn} higher than 350°C. These patterns are assigned to Ni/Ni$_3$Si/Ni$_{31}$Si$_{12}$ (T3; T_{syn}=350°C), Ni$_2$Si (T4; T_{syn}=400°C) and Ni$_2$Si/Ni$_3$Si$_2$ (T5 and T6(A1); T_{syn}=500 and 600°C).

In Figure 2(b), the XRD patterns for samples synthesized at fixed T_{syn} (600°C) with various α values in the range of 0.5-2.0 are shown. From the patterns for samples A7 (α=0.5), A6 (α=0.7) and A5 (α=1.0), Ni is found to be the reaction product. The intensity of the peaks corresponding to CaSi$_2$ (a raw substance) decreased as α increased from 0.5 (sample A7) to 1.0 (A3). Peaks associated with CaSi$_2$ were not observed from the patterns for samples synthesized with α higher than 1.0 (A4, A3, A2 and T6(A1)), whereas NiSi$_y$ became the major crystalline phases. The phase of NiSi$_y$ changed with increasing α as NiSi (A4; α=1.1) → NiSi/Ni$_3$Si$_2$ (A3; α=1.3) → NiSi/Ni$_3$Si$_2$/Ni$_2$Si (A2; α=1.6) → Ni$_3$Si$_2$/Ni$_2$Si (T6(A1); α=2.0).
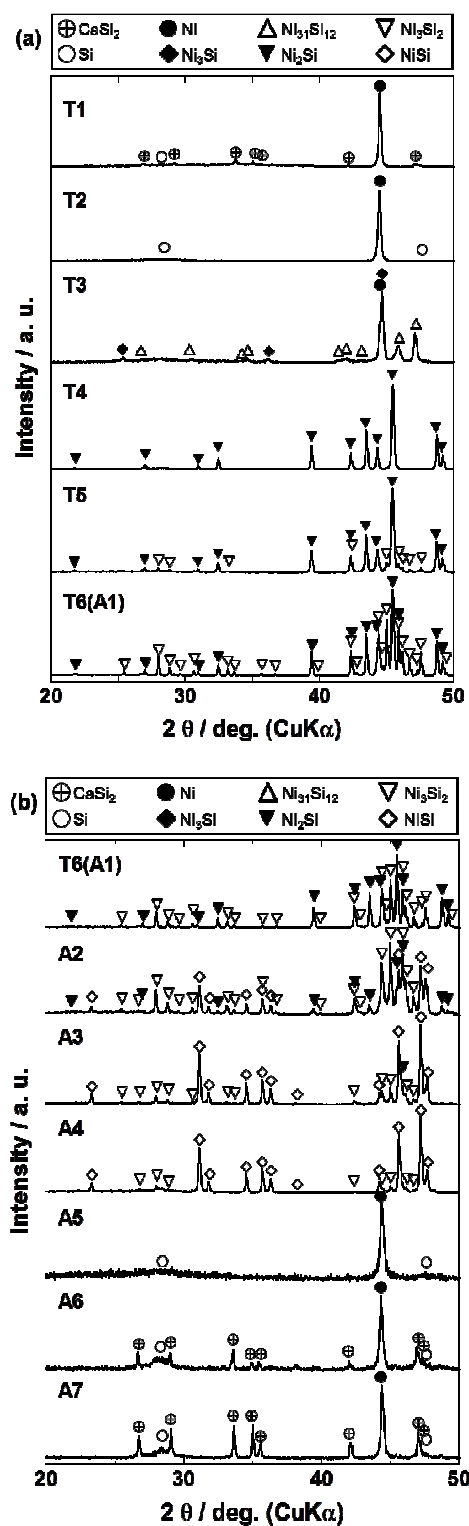
Figure 2. Powder XRD patterns for DMF-washed samples. (a) The patterns for the samples prepared by various synthesis temperatures (T_{syn}) with fixed molar ratio (α) of 2.00. (b) Patterns for samples prepared with various α with fixed T_{syn} at 600°C. T_{syn} was 250 (T1), 300 (T2), 350 (T3), 400 (T4), 500 (T5) and 600°C (T6(A1)), and α was 2.0 (T6(A1)), 1.6 (A2), 1.3 (A3), 1.1 (A4), 1.0 (A5), 0.7 (A6) and 0.5 (A7). NiSi ($\diamond$), Ni$_3$Si$_2$ ($\triangledown$), Ni$_2$Si ($\blacktriangledown$), Ni$_{31}$Si$_{12}$ ($\triangle$) and Ni$_3$Si ($\blacklozenge$) were referenced to JCPDS-ICDD PDF card #01-085-0901, #01-089-2906, #01-076-8258, # 00-017-0222 and # 01-077-9325, respectively.

Table 2. Components comprising the nanocomposites prepared by $\alpha NiCl_2/CaSi_2$ systems.

Sample	T_{syn} /°C	α^a / -	Reaction products						$CaSi_2$ (raw material)
			$Ca_xSi_2{}^b$	$NiSi^c$	$Ni_3Si_2{}^c$	Ni_2Si^c	Ni_3Si^c	Ni^c	
T1	250		Major					Major	minor
T2	300		Major					Major	
T3	350	2.0	minor			Major		minor	
T4	400					Major			
T5	500				minor	Major			
T6(A1)					Major	Major			
A2		1.6		minor	Major	minor			
A3		1.3		Major	Major	minor			
A4	600	1.1	minor	Major	minor				
A5		1.0	Major					Major	
A6		0.7	Major					Major	minor
A7		0.5	Major					Major	Major

note: a is molar ratio of $(NiCl_2/CaSi_2)$. b and c were identified by SEM-EDX and powder XRD analyses, respectively. $NiCl_2$ (raw material) in as-prepared sample T1 (before washing) was observed by powder XRD analysis. $CaCl_2$ in all as-prepared samples was removed by washing with DMF.

The materials identified by powder XRD and SEM-EDX analyses are summarized in Table 2. Because $CaCl_2$ co-existed in all samples before washing, it was considered that an exchange reaction between Ca of $CaSi_2$ and Ni of $NiCl_2$ would occur[10, 11]. As shown in Table 2, for the samples with a fixed α of 2.0, a Si-rich phase of $NiSi_y$ was formed as the major reaction product with increasing T_{syn} (in the order T3 < T4 < T5 < T6(A1)). It was expected that Ni from $NiCl_2$ and Si in Ca_xSi_2 would react, thereby forming $NiSi_y$. Acker et al. investigated the formation of nickel silicides with a kinetic model using thermodynamic equilibrium and an experimental study using isothermal powder XRD[13]. The solid-gas phase reaction was applied using a Ni-wire and a mixture of $SiCl_4/H_2$ gases as the source for Ni and Si, respectively. From both thermodynamic calculations and experimental results, it was shown that the Si-rich phase of $NiSi_y$ was formed as the reaction temperature increased. Their result on the phase selection of $NiSi_y$ is similar to that observed in this work, indicating that the Si-rich phase of $NiSi_y$ would be more stable than the Ni-rich phase at higher temperatures.

On the other hand, for the samples synthesized at 600°C, a part of the raw $CaSi_2$ retained due to an insufficient amount of $NiCl_2$ to complete the Ca-extraction from the layered $CaSi_2$. Ni was observed for sample A5 (α=1.0), whereas $NiSi_y$ was found for samples A4 (α=1.1), A3 (α=1.3), A2 (α=1.6) and T6(A1) (α=2.0). In addition, a Ni-rich phase of $NiSi_y$ was the major reaction product with increasing α (in the order of A4 < A3 < A2 < T6(A1)), suggesting that a larger amount of Ni in the reaction system would promote the formation of a Ni-rich phase of $NiSi_y$.

As a comparison of the $NiCl_2$ and $CaSi_2$ systems, samples were synthesized using '$FeCl_2$ and $CaSi_2$ (α=1.0, T_{syn}=600°C)' or '$MnCl_2$ and $CaSi_2$ (α=0.5, T_{syn}=600°C)'. As shown in the SEM images in Figure 3, the microstructures of the samples were similar to those of the samples synthesized by $NiCl_2$ and $CaSi_2$, i.e., the samples are agglomerated powders consisting of large particles with diameters more than 10 μm and small particles with diameters around 1 μm. SEM-EDX and powder XRD analyses suggested that the larger and smaller particles

were respectively Ca_xSi_2 particles and silicide particles of iron silicides (FeSi and Fe_3Si) or manganese silicides (MnSi and $MnSi_{1.73}$).

Even when $NiCl_2$ was replaced by $FeCl_2$ or $MnCl_2$, the synthesized samples before washing were found to contain $CaCl_2$. The standard enthalpy of formation at 600°C, $CaCl_2$, $NiCl_2$, $FeCl_2$ and $MnCl_2$, is reported to be -750, -260, -280 and -430 kJ mol^{-1}, respectively[14]. The formation of $CaCl_2$ would be the driving force for the reaction to proceed between the layered-$CaSi_2$ and '$NiCl_2$, $FeCl_2$ or $MnCl_2$'. Thus, the solid-state exfoliation reaction using layered-$CaSi_2$ and transition metal chlorides could yield nanocomposites containing various transition silicides other than nickel-, iron-, manganese silicides.
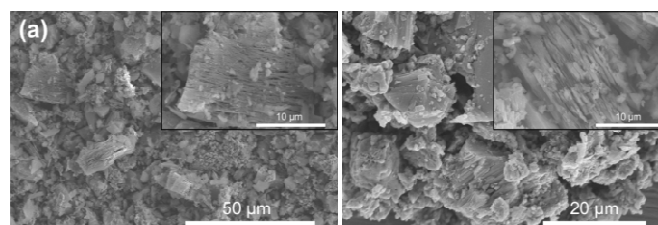
Figure 3. SEM images of samples prepared by (a) $\alpha FeCl_2 + CaSi_2$ (α=1.0, T_{syn}=600°C) and (b) $\alpha MnCl_2 + CaSi_2$ (α=0.5, T_{syn}=600°C) systems.

(2) Li-storage capacity and electrical conductivity of the nanocomposites

Figure 4 shows the initial capacity for samples A5 (α=1.0), A4 (α=1.1) and A3 (α=1.3) synthesized at 600°C as an anode in LIBs evaluated by the half-cell test. A5 showed a high capacity of 1,020 mAh g^{-1}, which is about 3 times higher than that of conventional graphite of 372 mAh g^{-1}. As shown in Figure 4, the discharge curves for the synthesized samples were similar to that for the Si anode, i.e., the discharge capacity was increased between 0.3-0.6 V (vs. Li/Li^+).

As shown in Table 2, samples A5 and A4 were formed as nanocomposites consisting of Ca_xSi_2 and Ni or $NiSi_y$, respectively, whereas sample A3 only contained $NiSi_y$. The amount of Ca_xSi_2 is expected to increase in the order A5>A4>A3. The Ni_2Si reagent powder barely reacted with Li (< 100 mAh g^{-1} in Figure 4). This result is corresponding to the previous report[15] showing that some transition metal silicides did not react with Li. Because Ca_xSi_2 would mainly contribute as a Li-storage site, the capacity for these samples reflects the amount of Ca_xSi_2 in the nanocomposites. Although rather high initial capacity value of $CaSi_2$ was reported[16], the $CaSi_2$ reagent powder showed low capacity value in the current evaluation conditions. The higher capacity of Ca_xSi_2 than $CaSi_2$ (Figure 4) suggests that the nano-flake structure of Ca_xSi_2 would enhance their reactivity with Li ions.

The pressure dependence of the electrical conductivity (σ) for the samples synthesized at 600°C with various α values in the range of 1.0-2.0 is shown in Figure 5. Sample A5 (α=1.0) exhibited low conductivity of 10^{-7} S cm^{-1} under all pressure loadings in the range of 2-15 MPa. It was found that the conductivity increased with increasing α, in the order of A5 (α=1.0)<A4 (α=1.1)<A3 (α=1.3)<A2 (α=1.7)<T6(A1) (α=2.0). The conductivity of samples A4, A3 and A2 increased as the loading pressure was increased from 2 to 15 MPa. In particular, sample T6(A1) exhibited a high conductivity of more than 0.1 S cm^{-1} under all loading pressures used.

As shown in Table 2, samples A5 and A4 are nanocomposites consisting of Ca_xSi_2 and 'Ni or $NiSi_y$' and sample A5 is expected to have a larger amount of Ca_xSi_2 than sample A4. In the case of sample A5, the amount of co-existing Ni was not sufficient to percolate to form conduction paths, thereby yielding a low σ of 10^{-7} S cm^{-1} under the entire loading pressure range of 2-15 MPa. On the other hand, sample A4 showed increased σ values with increasing loading pressure. Samples A3, A2 and T6(A1) showed higher σ values than samples A4 and A5, because the former samples are composed of only $NiSi_y$ particles with high σ values.
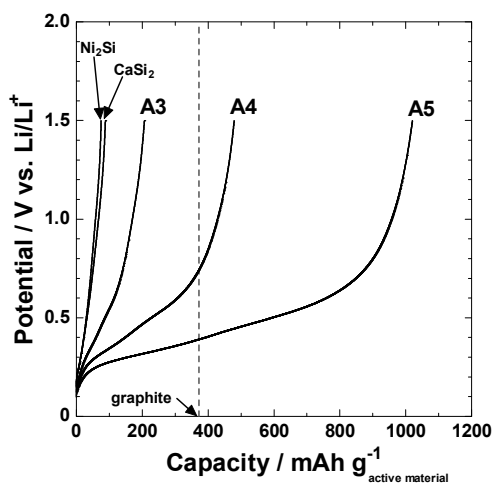
Figure 4. 1st discharge curves for the A5 (α=1.0), A4 (α=1.1) and A3 (α=1.3) samples synthesized at 600°C. The curves for $CaSi_2$ and Ni_2Si reagents are also presented for comparison.
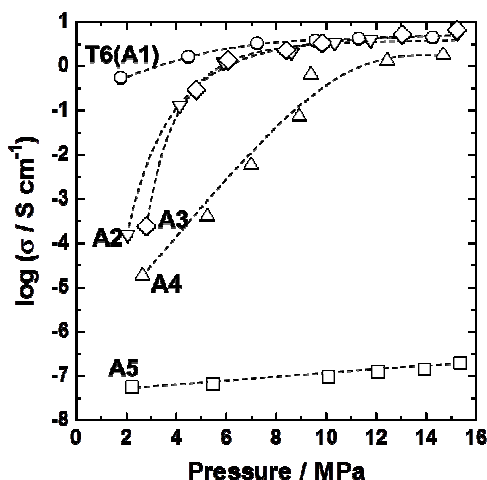
Figure 5. Pressure dependence of electrical conductivity for DMF-washed samples synthesized at 600°C. The symbols (□), (△), (◇), (▽) and (○) represent samples A5 (α=1.0), A4 (α=1.1), A3 (α=1.3), A2 (α=1.6) and T6(A1) (α=2.0), respectively. The dotted lines are included as a guide to the eye.
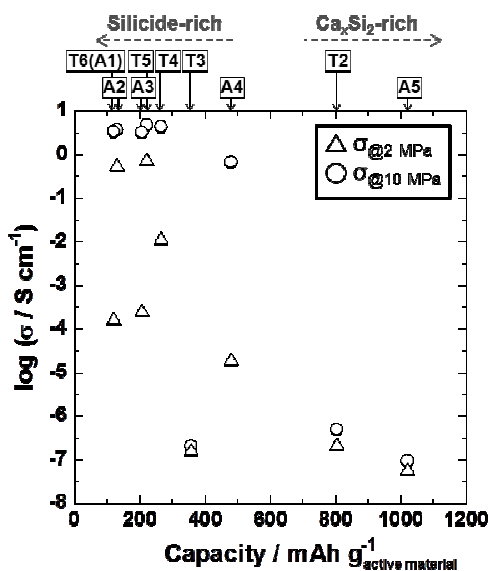
Figure 6. Correlation between electrical conductivity and 1st discharge capacity for samples of Ca_xSi_2/Nickel silicide nanocomposites.

Figure 6 shows the relationship between the discharge capacity in the 1st cycle and σ values of Ca_xSi_2/$NiSi_y$ nanocomposites. The σ values were data obtained at loading pressures of 2 (△) and 10 MPa (○). Here, the pressures of 2 and 10 MPa indicate the lowest limit of the load cell and pressure used to prepare electrodes for the half-cell test, respectively. Samples with a larger amount of Ca_xSi_2 in the nanocomposites showed higher discharge capacity with lower σ values. In reverse, the samples with smaller amounts of Ca_xSi_2 showed lower discharge capacity along with higher σ values. Among the synthesized samples in this study, the highest capacity of 1,020 mAh g^{-1} for sample A5 and the highest conductivity of 4.8 S cm^{-1} at 10 MPa for sample T6(A1) were achieved. These results indicate that the solid-state exfoliation reaction would indeed allow for the synthesis of nanocomposites with a tunable

mixing ratio of Ca_xSi_2 (Li-storage sites) and 'NiSi$_y$ or Ni' (conducting media). The higher σ values would be beneficial to transport of electrons thereby enhancing rate performances. Thus, the determination of the best balance of σ and capacity values of the nanocomposites along with optimizing electrode structures is important as a future study.

Conclusions

By the solid-state exfoliation reaction using layered $CaSi_2$ and $NiCl_2$, nanocomposites consisting of nano-flake structured Ca_xSi_2 (Li-storage sites) and nickel silicides (conducting media) with various mixing ratios were prepared. The amount of Ca_xSi_2 in the nanocomposites was varied over a wide range by simply varying only the synthesis temperature (T_{syn}) and molar ratio (α) of $CaSi_2$ and $NiCl_2$. Thus, the synthesized nanocomposites showed diverse characteristics in anode capacity for LIBs and electrical conductivity: $e.g.$, samples with respective values of 1,020 mAh g^{-1} and 6×10^{-8} S cm^{-1}, or with 479 mAh g^{-1} and 2×10^{-5} S cm^{-1} were prepared. In addition, the mixture of layered $CaSi_2$ and 'FeCl$_2$ or MnCl$_2$' was found to yield nanocomposites consisting of Ca_xSi_2 and 'iron silicides or manganese silicides'. These results suggest that the solid-state exfoliation reaction using layered $CaSi_2$ is a facile and scalable synthetic route to develop high performance Si-based nanocomposite anode materials.

Notes and references

^{a} Toyota Central Research & Development Labs., Inc., 41-1 Yokomichi Nagakute, Aichi 480-1192, Japan.

E-mail: *e1634@mosk.tytlabs.co.jp, **h-itahara@mosk.tytlabs.co.jp

† Electronic Supplementary Information (ESI) available: [The nitrogen adsorption isotherms and calculated specific surface areas for the prepared nanocomposites containing Ca_xSi_2]. See DOI:

1. U. Kasavajjula, C. Wang and A. J. Appleby, *Journal of Power Sources*, 2007, **163**, 1003-1039.

2. X. Su, Q. Wu, J. Li, X. Xiao, A. Lott, W. Lu, B. W. Sheldon and J. Wu, *Advanced Energy Materials*, 2014, **4**, 1300882.

3. H. Kim, B. Han, J. Choo and J. Cho, *Angewandte Chemie*, 2008, **47**, 10151-10154.

4. X. W. Lou, L. A. Archer and Z. Yang, *Advanced Materials*, 2008, **20**, 3987-4019.

5. Y. Yao, M. T. McDowell, I. Ryu, H. Wu, N. Liu, L. Hu, W. D. Nix and Y. Cui, *Nano letters*, 2011, **11**, 2949-2954.

6. D. Chen, X. Mei, G. Ji, M. Lu, J. Xie, J. Lu and J. Y. Lee, *Angewandte Chemie*, 2012, **51**, 2409-2413.

7. H. Wu, G. Chan, J. W. Choi, I. Ryu, Y. Yao, M. T. McDowell, S. W. Lee, A. Jackson, Y. Yang, L. B. Hu and Y. Cui, *Nat Nanotechnol*, 2012, **7**, 309-314.

8. J. K. Yoo, J. Kim, Y. S. Jung and K. Kang, *Adv Mater*, 2012, **24**, 5452-5456.

9. J. Sha, J. J. Niu, X. Y. Ma, J. Xu, X. B. Zhang, Q. Yang and D. Yang, *Advanced Materials*, 2002, **14**, 1219-+.

10. H. Itahara, T. Kobayashi, T. Ohsuna, T. Asaoka and Y. Saito, *Nanotechnology (IEEE-NANO; 2012 12th IEEE Conference)*, 2012, 1-4.

11. S.-Y. Oh, H. Imagawa and H. Itahara, 2014, **unpublished**.

12. H. Sakaguchi, T. Iida, M. Itoh, N. Shibamura and T. Hirono, *IOP Conference Series: Materials Science and Engineering*, 2009, **1**, 012030.

13. J. Acker, I. Rover, R. Otto, G. Roewer and K. Bohmhammel, *Solid State Ionics*, 2001, **141**, 583-591.

14. O. Knacke, O. Kubaschewski and K. Hesselmann, *Thermochemical properties of inorganic substances*, Springer-Verlag, Berlin, 1991.

15. M. D. Fleischauer, J. M. Topple and J. R. Dahn, *Electrochemical and Solid-State Letters*, 2005, **8**, A137.

16. J. Wolfenstine, *Journal of Power Sources*, 2003, **124**, 241-245.